

# This is not the feedback you have been looking for: nearby optical AGN rarely drive kpc-scale cold-gas outflows

Borislav Nedelchev<sup>1,2\*</sup>, Marc Sarzi<sup>1</sup> and Sugata Kaviraj<sup>1</sup>

<sup>1</sup>Center for Astrophysics Research, University of Hertfordshire, College Lane, AL10 9AB Hatfield, UK

<sup>2</sup>European Southern Observatory, Karl-Schwarzschild-Str. 2, 85748, Garching bei München, Germany

6 October 2018

## ABSTRACT

We study the interstellar Na I  $\lambda\lambda 5890, 5895$  (Na D) absorption-line doublet in a nearly-complete sample of  $\sim 9900$  nearby Seyfert 2 galaxies, in order to quantify the significance of optical AGN activity in driving kpc-scale outflows that can quench star formation. Comparison to a carefully matched sample of  $\sim 44,000$  control objects indicates that the Seyfert and control population have similar Na D detection rates ( $\sim 5 - 6\%$ ). Only 53 Seyferts (or 0.5% of the population) are found to potentially display galactic-scale winds, compared to 0.8% of the control galaxies. While nearly a third of the Na D outflows observed in our Seyfert 2 galaxies occur around the brightest AGN, both radio and infrared data indicate that star formation could play the dominant role in driving cold-gas outflows in an even higher fraction of the Na D-outflowing Seyfert 2s. Our results indicate that galactic-scale outflows at low redshift are no more frequent in Seyferts than they are in their non-active counterparts, that optical AGN are not significant contributors to the quenching of star formation in the nearby Universe, and that star-formation may actually be the principal driver of outflows even in systems that do host an AGN.

**Key words:** galaxies: elliptical and lenticular, cD – galaxies: spiral–galaxies: nuclei – galaxies : evolution

## 1 INTRODUCTION

Feedback from active galactic nuclei (AGN) is often invoked as a key mechanism for suppressing star formation in massive galaxies, where stellar winds and supernovae explosions are not sufficiently energetic to efficiently expel gas from their deep gravitational potential wells (e.g. Silk & Rees 1998). In such massive systems, the energy released when their supermassive black holes (SMBHs) accrete matter can exceed the gravitational binding energy of their host galaxies by several orders of magnitude. Thus, from a theoretical point of view, energetic feedback from AGN is thought capable of disrupting the progress of star formation in such systems, through the heating and ejection of the galaxy’s gas reservoir (Fabian 2012). Such (negative) AGN feedback is frequently incorporated in models of galaxy formation, to prevent the overprediction of over-massive systems in the models and bring their predicted properties, like colours, in line with observations (e.g. Croton et al. 2006; Scannapieco et al. 2012; Kaviraj et al. 2017).

From an empirical perspective, the AGN hypothesis is

qualitatively supported by the observed correlations between SMBH masses and various global physical properties of their host galaxies (e.g. velocity dispersion), which suggest that the host galaxy and its SMBH may grow in lockstep with each other (see King & Pounds 2015, for a review). Nevertheless, the detailed processes behind this possible coevolution (Kormendy & Ho 2013) remain unclear, and gaining insight into the impact that SMBHs can have on the evolution of their hosts in large statistical samples of galaxies is essential (Schawinski 2012).

The clearest examples of host-AGN interaction are arguably found in nearby brightest cluster galaxies. The AGN in these systems have been shown to deposit vast amounts of energy into the surrounding intracluster medium via heating and (mega-parsec scale) jets both observationally and by means of modeling (e.g. Binney 2004; Scannapieco et al. 2005; English et al. 2016; Gitti et al. 2012, for a review), which maintain the hot gas reservoirs in these systems, prevent cooling flows and thus suppress star formation (e.g. Binney & Tabor 1995; Li et al. 2015). In lower-density environments (where the majority of galaxies live), the empirical picture is much less clear. Direct observational evidence for AGN feedback on galactic scales in such environments

\* E-mail: b.nedelchev@herts.ac.uk

remains sparse. More specifically, while outflows have been detected in a number of instances around AGN in various gas phases, most of these detections have been made in ultra-luminous infrared galaxies or some of the closest quasar-host galaxies (e.g. Nyland et al. 2013; Rupke et al. 2005b; Harrison et al. 2014), with only a few examples where the AGN have been shown to couple with kpc-scale outflows that are capable of impacting star-formation on galactic scales (Cicone et al. 2014; Harrison 2017, for a review). Thus, it is still unclear to what extent the general AGN population could drive kpc-scale galactic outflows capable of limiting or quenching star-formation in the local Universe.

Indeed, some recent work has cast doubt on the ability of AGN (outside clusters) to strongly regulate star formation in the *nearby* Universe. These studies indicate that the time delay between the peak of the star formation and the onset of AGN activity is several dynamical timescales (Kaviraj et al. 2011, 2015; Shabala et al. 2017). Consequently, AGN couple mainly to residual gas, at a point where star formation has already declined and the original gas reservoir is already significantly depleted (Sarzi et al. 2016). This, in turn, makes it unlikely that the AGN play a significant role in regulating their associated star formation episodes. A fuller understanding of the role of AGN in regulating star formation demands a direct study of whether outflows of neutral material (which are ultimately responsible for quenching star formation) are more likely launched in AGN hosts. Most importantly, a quantitative statement about the putative role of AGN in influencing the evolution of their host galaxy requires a study that employs a complete sample of such AGN in the local Universe. Performing such an analysis is the purpose of this paper.

An efficient way to identify galaxies that are going through an outflow phase is to look for the presence of interstellar Na I  $\lambda\lambda 5890, 5895$  (Na D) absorption that is blue-shifted with respect to the systemic velocity of the galaxy. Indeed, the low-ionisation potential of Sodium makes the detection of blue-shifted Na D lines an unambiguous signature of neutral interstellar material that is being entrained within an outflow, observed against the stellar background of the host galaxy (Rupke et al. 2005a). In this paper we measure the incidence and kinematics of interstellar Na D absorption in one of the largest samples of nearby Seyfert 2 galaxies drawn from the Sloan Digital Sky Survey Abazajian et al. (2009), and compare these results with similar measurements obtained in a carefully selected control sample designed to match our Seyfert 2 galaxies in redshift, luminosity, size, light concentration, apparent flattening, colour and, when available, morphological classification into early or late type objects. We use this comparison to quantify whether the frequency of kpc-scale cold-gas outflows increases in Seyfert 2's, with a view to understanding the impact that the central engines of Seyfert 2 galaxies have on their hosts.

This paper is organized as follows. Section 2 gives a brief description of our Seyfert 2 sample, and the procedure used to construct the control sample. Section 3 describes how we identify and extract the kinematics of Na D absorption features. In Section 4 we present the results of this analysis and in Section 5 we summarize our conclusions.

## 2 DATA AND SAMPLE SELECTION

Both the analysis and the sample selection that underpins this work are based on Data Release 7 of the Sloan Digital Sky Survey (SDSS; Strauss et al. 2002; Abazajian et al. 2009). For our measurements of Na D line strength and position, we re-analyse the SDSS spectra that were used for the construction of the Oh et al. (2011) value-added SDSS catalogue (hereafter OSSY), which analysed in detail 664,187 galaxies at  $0.0 < z < 0.2$  and provides key quantities such as the value of the stellar velocity dispersion and the strength of nebular emission lines. The relative intensity of emission lines, as measured in OSSY, was also used to select our core Seyfert 2 sample and classify the nebular emission of our control objects by means of standard BPT diagnostic diagrams (Baldwin et al. 1981).

For measuring total luminosities and colours we obtain absolute, de-reddened, K-corrected magnitudes from the SDSS DR7 in the u- and r-band, that are based on the best-fitting de Vaucouleurs or exponential model magnitudes (*ModelMag*). The K-corrections are taken from the *kcrr* value for the u- and r-band listed in the SDSS *Photoz* table (O'Mill et al. 2011), whereas for computing absolute magnitudes we use the luminosity distance returned by the *fCosmoDl* functions in the SDSS *CfunBASE* library (Taghizadeh-Popp 2010) and the SDSS redshift listed in the *SpecObjAll* table. All necessary isophotal measurements for measuring the radial extent, flattening and concentration of the SDSS galaxies are taken from the SDSS *PhotoObjAll* table, in particular, the r-band values for the *isoA* and *isoB* measurements of the major- and minor-axis radii and the *petroR90* and *petroR50* entries for the Petrosian radii enclosing 90% and 50% of the Petrosian flux.

Finally, in this work, we consider only the OSSY catalogue objects that were visually inspected by the Galaxy Zoo citizen-science project (Lintott et al. 2011). Since around 94% of the OSSY catalogue objects were covered by Galaxy Zoo, the requirement of a visually-classified morphology does not significantly reduce the final sample of 625,607 objects from which we select the Seyfert 2 and control samples that underpin this study.

### 2.1 Seyfert 2 sample

As a starting point for selecting a sample of Seyfert 2 host galaxies, we select objects in the OSSY catalogue which had emission-line amplitude-to-noise ratios (A/N) greater than 3, for both the [O III] $\lambda 5007$  and [N II] $\lambda 6584$  forbidden emission lines and for the H $\alpha$  and H $\beta$  recombination lines. Such a detection threshold allows us to safely place them on the so-called BPT (Baldwin et al. 1981) emission-line diagnostic diagrams and, more specifically, on the one introduced by Veilleux & Osterbrock (1987) that combines the [N II]/H $\alpha$  and [O III]/H $\beta$  line ratios. We adopt the empirical demarcation of Kauffmann et al. (2003) to separate these galaxies into ones where the gas ionization is driven by star-formation (SF) activity and ones potentially driven by AGN. Furthermore, by applying the Kewley et al. (2001) maximum theoretical star-burst division line, we differentiate a class of galaxies with a superposition of AGN and star-formation activity (TO for “transition”). Finally, the rest of the emission-line galaxies with plausible AGN contributions

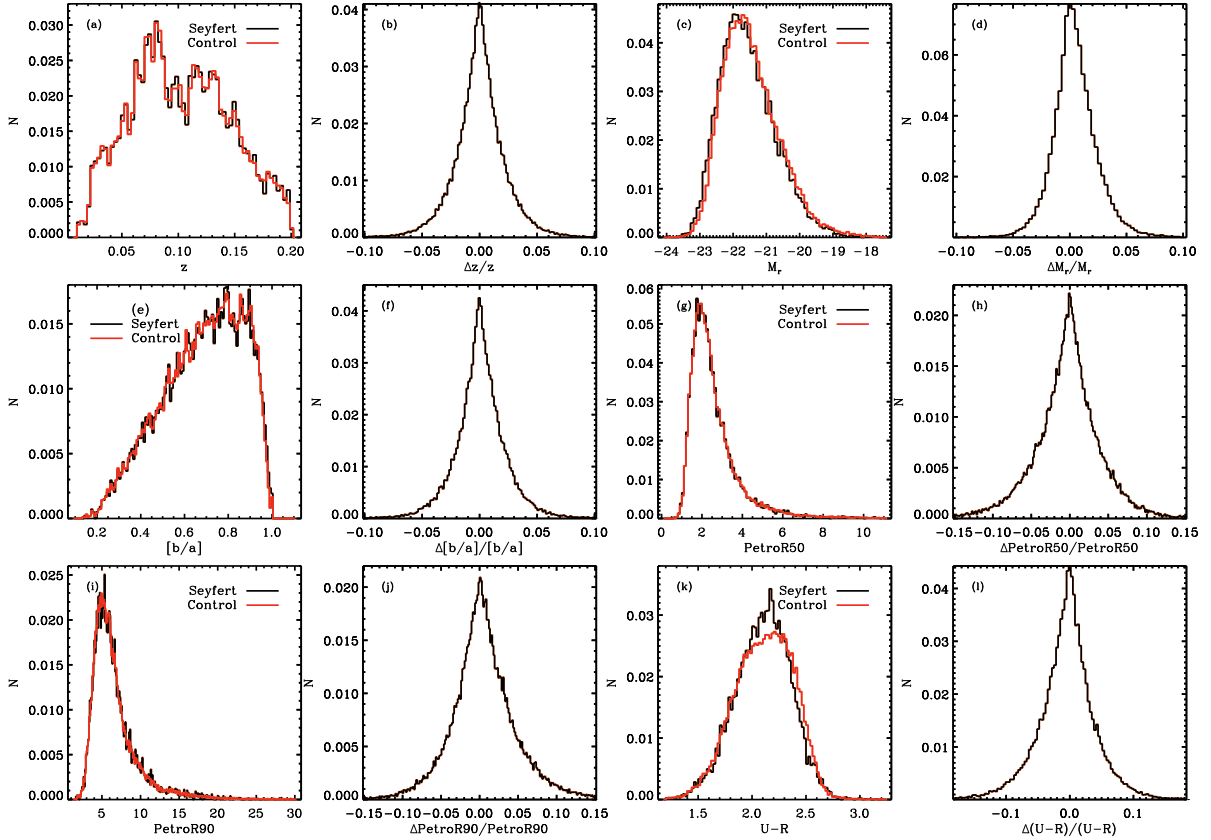


**Figure 1.** The result of our control matching procedure. Panels (a), (c), (e), (g), (i), (k) show the distribution of our Seyfert 2 and control samples in all parameters used in the matching process - redshift ( $z$ ), absolute r-band magnitude ( $M_r$ ), isophotal semi-minor and major ratio ( $[b/a]$ ), Petrosian radius containing 50% of the light ( $PetroR50$ ), Petrosian radius containing 90% of the light ( $PetroR90$ ), and the difference in the absolute magnitude in the u- and r-bands ( $U - R$ ). The remaining panels (b), (d), (f), (h), (j), (l) present the fractional difference between the aforementioned parameters for the galaxies in the control sample and the Seyfert 2 galaxy they match, normalised by the value of the corresponding parameter for the Seyfert 2. We achieve a good overall matching between the Seyfert 2 and control galaxy distribution, with the slight exception of  $U - R$  where our matching procedure produces slight differences near the peak of the colour distribution.

were divided on the basis of the empirical criterion developed in Schawinski et al. (2007), to isolate Seyfert galaxies (Sy) from the ones with low-ionization emission regions (LI), which can rarely be attributed to real AGN activity and are instead more often due to extended emission (Sarzi et al. 2010; Cid Fernandes et al. 2010, 2011; Yan & Blanton 2012; Singh et al. 2013; Belfiore et al. 2016). As a result of this selection process we arrive at an initial sample of 10,983 Seyfert galaxies. Since many of these Seyfert objects could potentially display broad-line regions (BLR), and a featureless AGN continuum that would considerably complicate our NaD measurements (Cardoso et al. 2017), we further restrict ourselves solely to *narrow-line* Seyfert 2 galaxies, by excluding the Type 1 Seyferts identified by Oh et al. (2015). This leaves us with a final sample of 9859 Seyfert galaxies.

## 2.2 Control Sample

In order to ascertain the importance of AGN in driving outflows, we will compare our NaD analysis of the Seyfert 2 sample, to an identical analysis on a carefully selected

sample of control galaxies. Following a procedure similar to Westoby et al. (2007), we proceed by finding, for each Seyfert 2 object in our sample, five control galaxies that are closest to the Seyfert in question in the following quantities:

- (i) Redshift,  $z$ , from the SDSS DR7 pipeline.
- (ii) Absolute r-band magnitude,  $M_r$ , K-corrected and de-reddened for the Galactic extinction, as described above. This is done to match galaxies as closely as possible in their total stellar luminosity.
- (iii) Apparent flattening,  $b/a$ , using the r-band isophotal minor- to major-axis ratio. For spiral galaxies, this quantity provides a useful measure of inclination.
- (iv) The radius containing 90% of the Petrosian flux,  $PetroR90$ , which, when combined with our  $z$  matching, enables us to match galaxies in their intrinsic size. This also ensures that the SDSS spectroscopic measurements encompass roughly the same fraction of galaxy light in our Seyfert 2 and control galaxies.
- (v) The radius containing 50% of the Petrosian flux,  $PetroR50$ , which, when combined with our  $PetroR90$



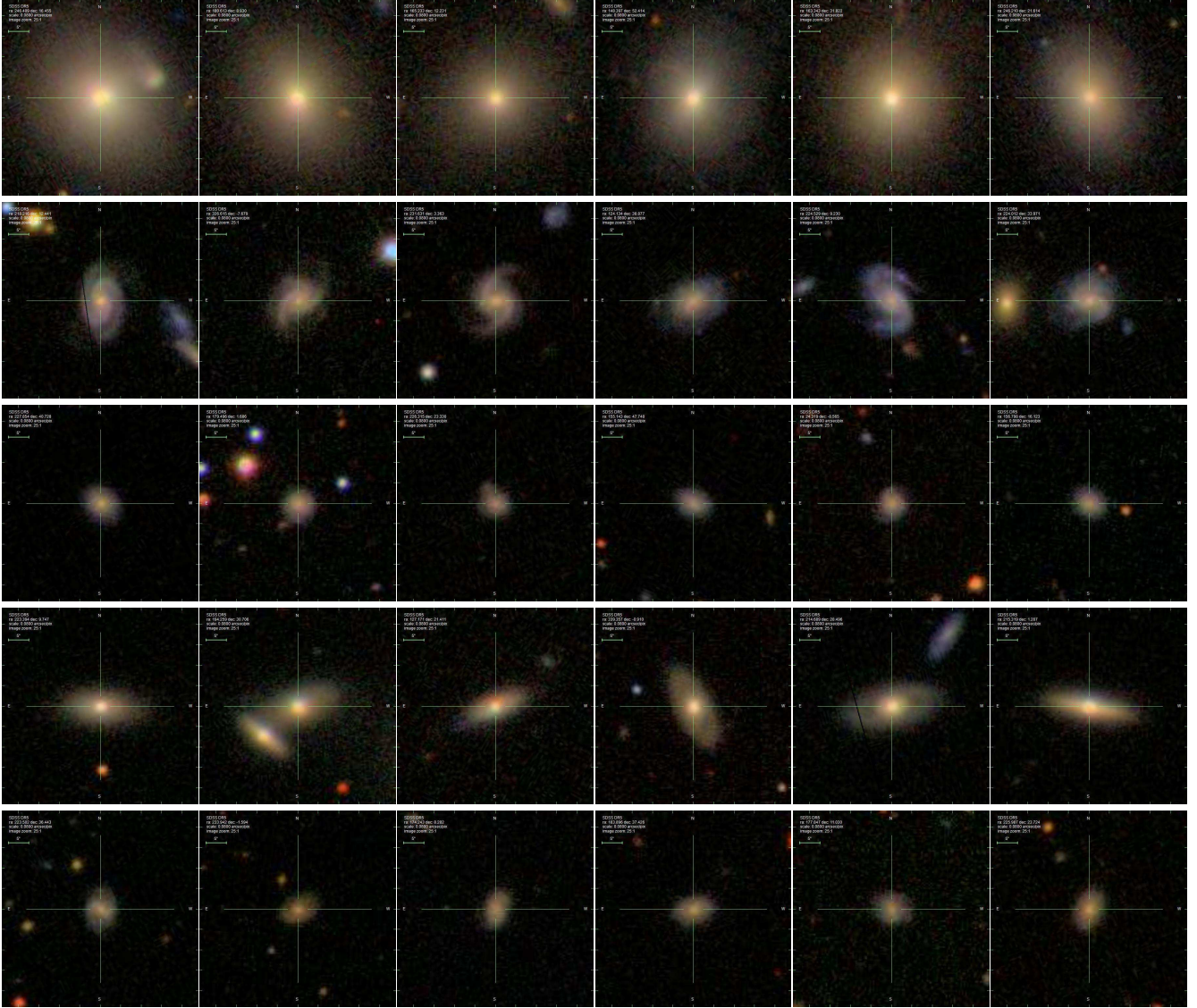


**Figure 2.** SDSS colour images for Seyfert and control galaxies in our study. The image in the first column is the Seyfert 2 galaxy in question, while the next four columns in the corresponding row are the five closest-matched control galaxies. The top two rows show morphologically matched early- and late-type objects, respectively. All other rows show the results of our matching procedure when morphological criteria cannot be used due to an “uncertain” classification in Galaxy Zoo for the Seyfert in question.

matching, allows us to match galaxies in their degree of light concentration. In the absence of a robust visual classification, this, to some extent, provides a proxy for the galaxy morphology (Shimasaku et al. 2001; Strateva et al. 2001).

(vi)  $U - R$  color, based on their  $M_u$  and  $M_r$  absolute magnitudes. Combined with our  $M_r$  matching, this allows us to pick objects with comparable positions in the  $M_r$  vs.  $U - R$  color-magnitude diagram, therefore selecting galaxies with similar star-formation rates and star formation histories.

To find the best control objects for each of our Seyfert 2 galaxies we decided against minimising the sum ( $\Delta C$ ) of the absolute differences in each matching parameter (e.g.,

$\Delta z$ ) as done for instance in Westoby et al. (2007) and opted instead to consider such differences in relative terms (i.e.  $\Delta z/z$ ) and weighting them as follows:

$$\Delta C = \frac{|\Delta z/z|}{0.05} + \frac{|\Delta M_r/M_r|}{0.1} + \frac{|\Delta [b/a]/[b/a]|}{0.05} + \frac{|\Delta \text{petroR90}/\text{petroR90}|}{0.1} + \frac{|\Delta \text{petroR50}/\text{petroR50}|}{0.05} + \frac{|\Delta (M_u - M_r)/(M_u - M_r)|}{0.1} \quad (1)$$

This allows us to find matching control objects more

precisely at the higher- and lower- end of the Seyfert 2 distribution for each of the previous parameters, and to assign a relative error meaning to our adopted weights. The weights themselves are chosen following an iterative process. Very broad initial constraints (i.e. asking all parameters to be not so precisely matched) were initially imposed and further tightened, guided by the specific number of available control galaxies for every Seyfert, in our parameters of interest, until our matching procedure achieved the relative best match across all six adopted parameters.

For each of our Seyfert 2 objects, we compute  $\Delta C$  for all OSSY galaxies, and then pick the five objects with the lowest  $\Delta C$  as control counterparts for the Seyfert in question. During this process, if a Seyfert 2 object had a robust ‘‘super-clean’’ Galaxy Zoo classification and was classified either as a spiral or an elliptical, we proceeded to find the best five control galaxies as done above, but while considering only OSSY objects that were also robustly classified to be of the same morphological type. This selection process results in 44,123 unique control galaxies. Fig. 1 shows how our matching process returns control galaxies, with parameter distributions that closely match the corresponding distributions for our Seyfert 2 sample (panels a, c, e, g, i, and k). Fig. 1 also shows how the values for these parameters for the five best control galaxies are generally within 5 to 10% of the ones of their parent Seyfert 2 objects (panels b, d, f, h, j, and l), broadly consistent with the weighting applied in Eq. (1). The only exception in this respect concerns our colour matching, since the  $U - R$  distributions for our Seyfert 2 and control sample differ slightly near their peaks and red tails.

Fig. 2 further illustrates the quality of our control sample selection, by presenting SDSS colour composite images for 5 randomly selected Seyfert 2 galaxies (left column) and their respective five best controls (columns to the right). In Fig. 2 the top two rows are Seyfert 2 galaxies that are classified by Galaxy Zoo as an elliptical and spiral respectively. Conversely, the last three rows show how our matching process returns control galaxies that look similar to our Seyfert 2 objects even when the morphology of the latter was classified as ‘uncertain’ by Galaxy Zoo.

### 3 ANALYSIS

To assess the presence of interstellar NaD absorption, and measure the kinematics of these lines, we closely follow the procedure described in Sarzi et al. (2016):

(1) We normalise the SDSS spectra in the NaD region using the best-fitting stellar continuum, obtained using the pPKF and GandALF spectral fitting codes (Cappellari & Emsellem 2004; Sarzi et al. 2006), with the synthetic stellar population (SSP) of Bruzual & Charlot (2003) used as stellar templates. This fitting is entirely consistent with the one carried out during the compilation of the OSSY catalogue, except that in this work we avoid using the semi-empirical templates that were constructed by Oh et al. (2011) in order to better match the spectra of massive early-type galaxies. Matching the nebular emission in this process is critical to account also for the possible presence of He I  $\lambda 5875$  emission.

(2) After normalising the SDSS spectra, we fit the resulting NaD absorption profile using the parametrisation given by Sato et al. (2009):

$$I(\lambda) = 1 - C_f \left\{ 1 - \exp \left[ - 2\tau_0 e^{-(\lambda - \lambda_{\text{blue}})^2 / (\lambda_{\text{blue}} b/c)^2} - \tau_0 e^{-(\lambda - \lambda_{\text{red}})^2 / (\lambda_{\text{red}} b/c)^2} \right] \right\} \quad (2)$$

where  $C_f$  is the covering factor of the absorbing cloud complex,  $\tau_0$  is the optical depth at the centre of the red NaD line,  $\lambda_{\text{blue}}$ ,  $\lambda_{\text{red}}$  are the red- or blue- shifted wavelengths of the two NaD lines, and  $b_D = \sqrt{2}\sigma_{\text{NaD}}$  is the Doppler parameter. The red- or blue- shifted central-line values and  $b_D$  yield the quantity of interest here, namely the velocity  $V_{\text{NaD}}$  and the width  $\sigma_{\text{NaD}}$  of the NaD lines.

The procedure mentioned above assumes a single velocity distribution for the absorbing gas clouds along the line of sight<sup>1</sup>. However, this may not be accurate for galaxies that host both a significant ‘‘systemic’’ population of absorbers settled in the galaxy plane and a population of outflowing clouds, in particular, when looking at these objects from an intermediate inclination angle (Chen et al. 2010). While this approach would lead us to underestimate the outflow velocity in galaxies that are viewed from intermediate inclination angles, using a single NaD velocity profile will suffice to capture the kinematic behaviour of the cold gas across tens of thousands of Seyfert 2 and control galaxies and, most noticeably, to estimate and compare the fractions of objects that could display cold-gas outflows in our samples.

As noted in Sarzi et al. (2016), one has to be aware that after normalising the SDSS spectra, an NaD absorption excess could also be the result of template mismatch, for instance in the case of objects with an enhanced [Na/Fe] abundance in their stellar population that is not accounted by our adopted SSP template library (Jeong et al. 2013; Park et al. 2015). Fortunately, objects where the NaD excess is entirely artificial (in the context of our procedure) can be isolated using the OSSY values for the  $E(B - V)$  that affects the entire spectrum (as opposed to reddening that impacts just the nebular emission, Jeong et al. (2013)). In other words, very small values of  $E(B - V)$  allow us to identify objects with little or no interstellar medium.

To restrict our study to objects displaying an NaD excess that is truly due to interstellar medium (ISM) absorption, as opposed to template-mismatch, we therefore select objects with  $E(B - V) > 0.05$ . This threshold appears to separate well the main Gaussian distribution of  $E(B - V)$  values across both our Seyfert and control samples from the offset peak of quiescent galaxies with zero or very small  $E(B - V)$  values.

Finally, to define a detection threshold for an NaD absorption excess in the SDSS data, we run our NaD fitting procedure through a large number of simulated spectra, obtained by adding random noise and an artificial NaD absorption profile to the best-fitting stellar population model. By exploring how well the input NaD parameters and, in particular,  $V_{\text{NaD}}$  and  $\sigma_{\text{NaD}}$ , are recovered as a function of

<sup>1</sup> More specifically, it assumes a Maxwellian velocity distribution for the gas clouds and that the covering fraction  $C_f$  is itself independent of the clouds’ velocities.



Emission class	all	with Na D	Na D outflows
Seyfert	9859	561 (5.7%)	53 (9.4%)
control	44123	2174 (4.9%)	352 (16.2%)
control-SF	6710	587 (8.7%)	92 (15.7%)
control-TO	5895	567 (9.6%)	147 (25.9%)
control-LINER	859	105 (12.2%)	27 (25.7%)
control-NE	30659	915 (2.9%)	87 (9.5%)

**Table 1.** Breakdown of our Seyfert 2 and control samples, according to whether or not interstellar NaD absorption was detected (third column, for objects with  $A/N_{\text{Na D}} > 4$  and  $E(B - V) > 0.05$ , see § 3) and furthermore if it likely traces outflows (fourth column, for object with  $\Delta V = V_{\text{Na D}} - V_{\star} < -100 \text{ km s}^{-1}$ , see § 4.1). Control galaxies are further subdivided according to their emission-line classification either as star-forming regions (SF), composite AGN/star-forming activity (TO), low-ionisation - possibly truly nuclear - emission regions (LI), or displaying little to no emission (NE). Percentages in the third column refer to the fraction of NaD-outflowing objects with respect to the number of objects with detected NaD interstellar absorption (third column).

the observed  $A/N_{\text{Na D}}$  ratio between the peak amplitude of the NaD profile and the input noise level, we conclude that at least  $A/N_{\text{Na D}} > 4$  values are required to secure unbiased  $V_{\text{Na D}}$  and  $\sigma_{\text{Na D}}$  measurements. This is consistent with the  $A/N > 4$  threshold estimated by the simulations of Sarzi et al. (2006) for ionised-gas emission lines with Gaussian profiles (in their case for the [O III] $\lambda\lambda 4959, 5007$  doublet), which can be understood considering that the NaD interstellar absorption profile can also be matched by means of two negative Gaussians of identical redshift and width in the low optical-depth regime where the NaD absorption is weak and NaD lines are far from saturating.

## 4 RESULTS

We begin by discussing the incidence and kinematics of NaD interstellar absorption in our control sample, while also defining the NaD blue-shift threshold that identifies outflowing systems (§ 4.1). We then compare these results with what is observed in our Seyfert 2 sample (§ 4.2). However, before conclusions can be drawn from such a comparison, it is important to first consider the incidence of interstellar NaD absorption in both the control and Seyfert 2 samples. Tab. 1 shows that the fraction of Seyfert 2 objects where NaD interstellar absorption is detected (5.7%) is consistent with that of control galaxies (4.9%).

Such a remarkable similarity, combined with our careful control sample construction, allows us to directly compare the NaD kinematics in our two samples and to reflect on the importance of AGN feedback. In particular, this finding goes against the argument that the AGN in the Seyfert 2 galaxies would substantially ionise its surroundings, as reported for instance by Villar Martín et al. (2014) for their sample of bright type 2 quasars. The ionising action of the AGN would indeed reduce the incidence of NaD interstellar absorption among our Seyfert 2s and thus limit the usefulness of the NaD lines as a tracer of cold-gas large-scale outflows only to objects with a faint AGN, which may not be able to provide much energetic feedback.

### 4.1 Control Sample

Tab. 1 shows that the majority (69%, or 30,659 out of 44,128 objects) of our control galaxies exhibit no or very weak nebular emission, with most remaining objects being almost evenly split between star-forming (13%) and composite (13%) nebular emission, plus a minority (3%) of galaxies displaying LINER-like emission. Tab. 1 also shows that the incidence of interstellar NaD absorption is around 9 – 12% for control galaxies with detected ionized-gas emission, dropping to just 3% among quiescent objects, which is consistent with the weak or absent nebular emission in these systems.

To understand the kinematics of interstellar NaD absorption in our control sample, we start by considering the top left panel of Fig. 3, where the velocity  $V_{\text{Na D}}$  and velocity dispersion  $\sigma_{\text{Na D}}$  of the NaD absorption is compared to the galaxy’s systemic velocity and central velocity dispersion ( $V_{\star}$  and  $\sigma_{\star}$  respectively). The colour-coding indicates the reddening by dust,  $E(B - V)$ . In this  $V_{\text{Na D}} - V_{\star}$  versus  $\sigma_{\text{Na D}} - \sigma_{\star}$  diagram, we observe the same trend as that observed in Sarzi et al. (2016), in that a majority of objects with nearly zero (or even slightly positive)  $V_{\text{Na D}} - V_{\star}$  ( $\Delta V$ ) and negative  $\sigma_{\text{Na D}} - \sigma_{\star}$  ( $\Delta\sigma$ ) values is followed by a long tail of galaxies with increasingly blue-shifted and broad NaD profiles, i.e. with progressively negative  $\Delta V$  and increasing  $\Delta\sigma$  values.

The bulk of the objects with  $\Delta V \sim 0$  consists of control galaxies where the NaD profile traces material that is likely settled in a dusty disk which is dynamically colder than the stellar bulge (thus corresponding to  $\Delta\sigma < 0$  values), or of highly-inclined systems where it would be hard to detect possible outflows. Conversely, detecting outflows and increasingly blue-shifted NaD lines is facilitated by looking at more face-on galaxies, where broad NaD profiles are also expected, as the line of sight intersects a multitude of cold-gas clouds moving at different velocities within large-scale bi-conical galactic winds (Fujita et al. 2009; Krumholz et al. 2017). Visual inspection of our control galaxies combined with using the inclination values derived from the axis ratio of late-type galaxies (51% of our control sample) confirms that the observed  $\Delta\sigma$  vs  $\Delta V$  anticorrelation is mainly driven by galaxy inclination. This trend is supported by the systematically higher  $E(B - V)$  values among low- $\Delta V$  objects, as would be expected for nearly edge-on dusty systems (Untertorn & Ryden 2008; Masters et al. 2010).

We proceed to address when NaD outflows are likely to occur in our control galaxies, by studying the distribution of values for their NaD velocity offset ( $\Delta V$ ), as shown in the top right panel of Fig. 3. The  $\Delta V$  distribution is skewed toward negative values (with a statistical skewness value of  $\sim -1.42$ ) and has a pronounced tail of objects with blue-shifted NaD interstellar absorption profiles. Yet, as stated before, the bulk of the control objects in Fig. 3 shows  $\Delta V \sim 0$  values, so that a Gaussian fit to the entire  $\Delta V$  distribution captures the distribution of the majority of these galaxies well, and allows us to isolate the tail of control objects that have NaD outflows. Observing that the control galaxies with  $\Delta V < -100 \text{ km s}^{-1}$  (the  $\sim 16^{\text{th}}$  percentile of the overall  $\Delta V$  distribution) already lie outside the region occupied by 90% of the objects enclosed by the fitted Gaussian (which has a FWHM of  $45 \text{ km s}^{-1}$ ), we consider this  $\Delta V$  threshold to be a conservative estimate for the start of

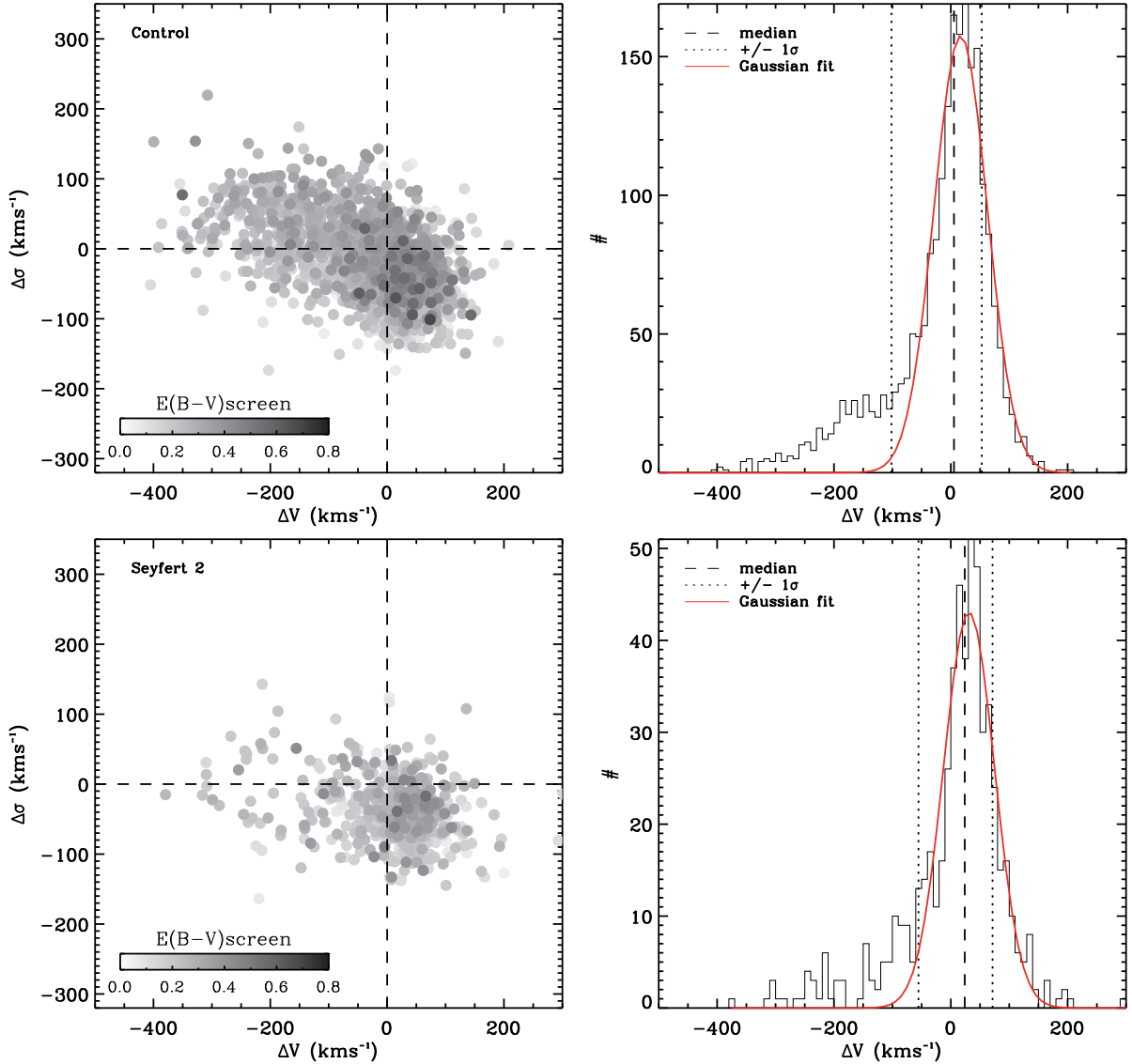


**Figure 3.** Kinematics of the NaD absorption component relative to the systemic properties of the galaxy, for our control and Seyfert 2 sample, where the observed NaD excess can be safely attributed to interstellar absorption. **Top left:**  $V_{\text{NaD}} - V_*$  ( $\Delta V$ ) versus  $\sigma_{\text{NaD}} - \sigma_*$  ( $\Delta\sigma$ ) for our control sample, colour-coded by the dust reddening  $E(B - V)$ . Only galaxies with  $A/N > 4$  for the NaD absorption and with  $E(B - V) > 0.05$  are shown (see text for more details). **Top right:** Histogram showing the distribution of the velocity offsets  $\Delta V = V_{\text{NaD}} - V_*$  for all the control galaxies shown in the top-left panel. The dashed line indicates the median of the distribution, and the dotted lines correspond to the  $\pm 1\sigma$  levels containing 68% of the  $\Delta V$  distribution. The red line shows the best-fitting Gaussian to the underlying distribution and emphasises the pronounced tail of galaxies with a  $\Delta V < -100$ . **Bottom left:** An identical  $\Delta V$  vs.  $\Delta\sigma$  diagram as in the top-left panels, but now for our Seyfert 2 sample. **Bottom right:** An identical  $\Delta V$  distributions as in the top-right panels, but now for our Seyfert 2 sample.

the tail of blue-shifted NaD control objects. Consequently, we consider galaxies with  $\Delta V < -100 \text{ km s}^{-1}$  as being likely to host cold-gas outflows, which are expected to be on kpc-scales given that at the mean redshift of our sample ( $z \sim 0.1$ ) the  $3''$  SDSS fibers subtend a region 5.5kpc across.

Among the control galaxies with detected NaD interstellar absorption, around  $\sim 16.2\%$  (Tab. 1) display NaD profiles blue-shifted by more than  $100 \text{ km s}^{-1}$ , which amounts to  $\sim 0.8\%$  of the control sample and is consistent with the overall outflow detection rate found in Sato et al.

(2009). Interestingly, we find that NaD outflows are not found most commonly in the star-forming objects (which host 16% of outflowing objects). Instead, outflows seem to be produced more efficiently in galaxies with either central composite AGN/star-forming or LINER-like emission (in 25% of the cases). Outflows are also traced in quiescent control objects with NaD interstellar absorption (10% of the cases) that generally display weak emission and where reddening prevented, in particular, the detection of [O III]. As such, the upper-limits on the [O III]/H $\beta$  line ratio indicates the pres-

ence of star formation or composite AGN/star-formation activity in most of these quiescent objects.

To study the role of star formation in driving outflows and further ascertain when it most likely powers them, it is instructive to look into the infrared (IR) luminosity of our control sample. For instance, it is well established that more than 50% of all luminous infrared galaxies (LIRGs) or ultraluminous infrared galaxies (ULIRGs) have blue-shifted NaD profiles indicative of outflowing gas (Heckman et al. 2000; Rupke et al. 2002, 2005a,b; Martin 2005).

To estimate the IR luminosities ( $L_{IR}$ ) of our control galaxies with NaD interstellar absorption, we employ the Ellison et al. (2016) catalog of predicted infrared luminosities for galaxies in the SDSS DR7, selecting only objects where the expected error in their infrared luminosity estimate is less than 0.1 dex. Among our control objects with interstellar Na D detection, 1519 (70%) have  $L_{IR}$  values from Ellison et al., and around 30% (461) of these have  $L_{IR} > 10^{11} L_{\odot}$  that would identify them as LIRGs or even ULIRGs. The fraction of objects with  $L_{IR} > 10^{11} L_{\odot}$  is substantially higher for objects with NaD outflows, being around 55% (148 objects out of 268), whereas for the bulk of our control objects that have  $\Delta V \sim 0 \text{ km s}^{-1}$  the fraction of objects with  $L_{IR} > 10^{11} L_{\odot}$  drops to 25% (313 out of 1251).

A higher incidence of U/LIRGs amongst our NaD-outflowing control objects is consistent with many of them being powered by star-formation, even though only 36 out of these 148 NaD-outflowing and IR-bright control objects are found in galaxies with star-forming central regions. This may suggest either that circum-nuclear star formation is driving the outflow or that, in many of these objects, shocks in the outflow lead to a more complex emission-line spectrum, as found in Ho et al. (2014), which could be recognised as LINER-like or composite AGN/star-forming emission (as found in 56% of the NaD-outflowing and IR-bright objects). In fact, shocks may also help explain why, more generally, NaD outflows are often associated with composite or LINER-like emission in our control galaxies, which can also be observed in the NaD kinematic analysis of the Jeong et al. (2013) sample by Park et al. (2015, see their Fig. 4).

## 4.2 Seyfert 2 sample

As noted above, the fractions of Seyfert and Control objects with interstellar NaD absorption are very similar, which is important, as this allows us to compare the cold-gas kinematics and, in particular, the incidence of NaD outflows in our two samples.

We proceed by studying the kinematics of the interstellar NaD lines in our Seyfert sample. The bottom left panel of Fig. 3, which shows the same  $\Delta V$  vs.  $\Delta\sigma$  diagram that we previously discussed for our control galaxies, indicates that among our Seyfert sample there is also a population of galaxies with blue-shifted NaD interstellar lines (e.g. with  $\Delta V < 0$ ) that are likely tracing outflowing material. The  $\Delta V$  distribution for our Seyfert 2 sample (bottom right panel of Fig. 3) shows a skewed distribution (with a statistical skewness  $\sim -1.22$ ), similar to that observed in the control sample, with a tail of objects with  $\Delta V < -100 \text{ km s}^{-1}$  extending away from the bulk of the systems that

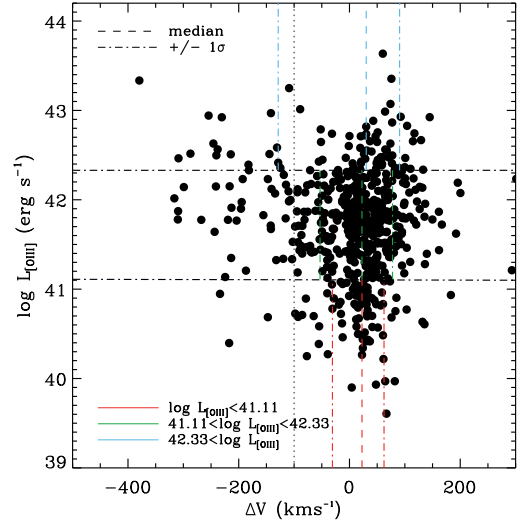


**Figure 4.** Dependence of the velocity shift  $\Delta V = V_{\text{NaD}} - V_{\star}$  on the AGN bolometric luminosity, as traced by  $\log L_{[\text{O III}]}$ , which, in turn, is derived from the extinction-corrected  $[\text{O III}]$  flux provided by the OSSY catalogue. The horizontal dashed-dotted lines indicate the ( $\pm 1\sigma$ ) 16% and 84% percentiles of the  $\log L_{[\text{O III}]}$  distribution. In each of the three  $\log L_{[\text{O III}]}$  regions defined by these  $\pm 1\sigma \log L_{[\text{O III}]}$  limits, the vertical dashed and dashed-dotted lines show the median and the  $\pm 1\sigma$  values for the velocity shifts  $\Delta V$ , respectively. Finally, the gray vertical dotted lines indicate our  $\Delta V = -100 \text{ km s}^{-1}$  threshold for identifying NaD outflows, as derived from our control sample (see text in § 4.1). Only at the highest  $\log L_{[\text{O III}]}$  end does the  $\Delta V$  distribution become significantly skewed, with a tail of outflowing objects. These objects comprise the most luminous  $\sim 20\%$  of Seyfert 2 galaxies, and 32% of all NaD-outflowing Seyfert 2 objects.

have nearly zero or slightly positive  $\Delta V$  values. Compared to the control sample, however, the tail of objects with blue-shifted NaD profiles is less pronounced, as it contains 9.4% of all Seyfert 2 galaxies with interstellar NaD absorption (compared to 16.2% for the control galaxies), corresponding to 0.53% of the overall Seyfert 2 sample (i.e. those with and without NaD absorption).

Given that the overall incidence of NaD-outflowing systems is similar to that found in our control sample, it is important to recall that our sample of 9859 Seyfert 2 galaxies offers a near complete view of the Seyfert 2 population within the footprint of the SDSS survey. Finding only 53 of such objects with kpc-scale cold-gas outflows already suggests that optical AGN activity cannot be important in driving galactic winds and quenching star-formation in the nearby Universe, even accounting for the fact that some more NaD-outflowing systems may have remained undetected in inclined Seyfert 2 galaxies. In fact, the role of AGN feedback may be even smaller considering how well connected Seyfert 2 and star-formation activity are (e.g., Kauffmann et al. 2003), so that circumnuclear star formation may also play a part in driving the NaD outflows that we observe in our Seyfert 2 sample.

To further quantify the importance of AGN feedback we check if the radiative power output of the AGN, i.e. its bolometric luminosity as traced by the extinction-corrected luminosity of the  $[\text{O III}]$  emission line (Lamastra et al. 2009), correlates with the velocity offset  $\Delta V$  of the interstellar NaD



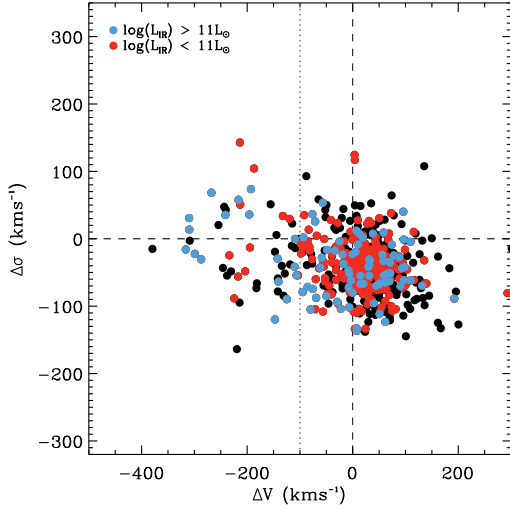


**Figure 5.**  $\Delta V$  vs.  $\Delta\sigma$  for Seyfert 2 galaxies with interstellar NaD absorption, similar to the one in Fig. 3 but now showing the objects colour-coded with IR luminosity estimates from the catalogue of Ellison et al. (2016). Blue and red points indicate galaxies with IR luminosities above and below the  $L_{IR} = 10^{11}L_{\odot}$  threshold i.e. LIRGs and ULIRGs respectively. Among the outflowing Seyfert 2 galaxies (i.e. those to the left of the grey vertical dotted line that marks our  $\Delta V = -100$  threshold for identifying NaD outflows, see § 4.1) 60% would be classified as LIRGs or ULIRGs.

absorption. This is shown in Fig. 4, where we find a modest tendency for galaxies with higher values of [O III] luminosity ( $\log L_{[O III]}$ ) to display blue-shifted interstellar NaD profiles (indicative of an outflow) more often. The fraction of NaD-detected Seyfert 2 galaxies where  $\Delta V < -100 \text{ km s}^{-1}$  indeed increases from  $\sim 3\%$  or  $\sim 9\%$ , for objects with low to intermediate [O III] luminosities, to  $\sim 19\%$  for the most luminous Seyfert 2 nuclei. Outflows are not predominantly found in such bright AGN (where we find  $\sim 32\%$  of the outflows), however, and inclination biases can also be excluded as we do not find - at least for Seyfert 2 in late-type galaxies (which are 38% of the Seyfert 2 hosts) - a correlation between axis ratio and [O III] luminosity.

If the weak trend shown by Fig. 4 could still be interpreted as evidence for AGN feedback in our NaD-detected Seyfert 2, one also has to keep in mind that the luminosity of the [O III] line in AGN is found to correlate with the star-formation rate of the host galaxy (LaMassa et al. 2013).

To check whether star-formation is possibly also driving the NaD outflows observed in our Seyfert 2 sample, we draw again from the work of Ellison et al. (2016) and look for the incidence of LIRGs or ULIRGs among our Seyfert 2 galaxies. This is illustrated by Fig. 5, where we present the same  $\Delta V$  vs.  $\Delta\sigma$  diagram for the NaD-detected Seyfert 2s as in Fig. 3, but now highlighting objects with  $L_{IR}$  above and below  $L_{IR} = 10^{11}L_{\odot}$ , which is the LIRG threshold. The Ellison et al. catalogue provides  $L_{IR}$  estimates for 308 (55%) of our Seyferts with NaD interstellar absorption, and of these, around 28% (88) are sufficiently IR-bright to be classified as LIRGs or ULIRGs. Among objects with  $L_{IR}$  estimates, the fraction of NaD-outflowing Seyferts (i.e. with  $\Delta V < -100 \text{ km s}^{-1}$ ) with  $L_{IR} > 10^{11}L_{\odot}$  is substantially higher than for Seyferts that show little or no evidence

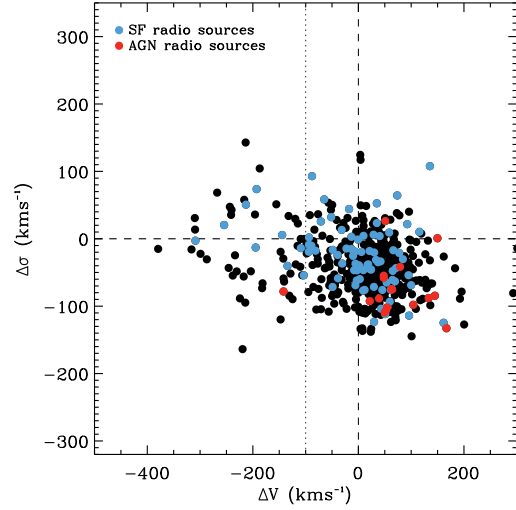


**Figure 6.**  $\Delta V$  vs.  $\Delta\sigma$  for Seyfert 2 galaxies with interstellar NaD absorption, similar to the one Figs. 3 and Fig. 5, but now showing radio sources that Best & Heckman (2012) associate with either AGN activity (red points) or star formation (blue points). Among the ten outflowing Seyfert 2 galaxies whose radio emission was classified in this way by Best & Heckman, only one is considered by these authors as being powered by a central AGN.

of cold-gas outflows (i.e. with  $\Delta V > -100 \text{ km s}^{-1}$ ), with these fractions being 60% (17 out of 28) and 25% (71 out of 280), respectively. The incidence of LIRGs or ULIRGs among NaD-outflowing Seyfert 2s is thus nearly twice as that of bright AGNs (32%), suggesting that circumnuclear star formation could indeed be driving many of the outflows observed among our Seyfert 2 galaxies. In fact, this possibility appears even more likely when considering that the fraction of IR-bright NaD-outflowing Seyfert 2s is also remarkably consistent with the corresponding value for the NaD-outflowing control objects (55%, § 4.1).

To further probe the relative role of AGN and star-formation in driving NaD outflows, we appeal to ancillary radio data for our galaxies. In particular, we employ the Best & Heckman (2012) radio catalogue of SDSS galaxies, where the presence of radio emission in each galaxy is linked to either star-formation activity or a radio-AGN, using their stellar-population properties, the ratio of the radio-to-optical-emission luminosity and standard BPT diagnostic diagrams. Fig. 6 again shows the  $\Delta V$  vs.  $\Delta\sigma$  diagram for our NaD-detected Seyfert 2 galaxies, where the coloured points now indicate whether the radio emission is dominated by star-formation or AGN activity. The Best & Heckman catalog includes 97 (19%) of our Seyfert 2 sample with interstellar NaD absorption and, out of these objects, the radio emission is ascribed to a radio AGN only in 17 objects (18%). Most importantly Fig. 6 shows that, among the ten radio-detected Seyfert 2 that also exhibit an NaD-outflow, only one is classified as a radio AGN by Best & Heckman. Radio-AGN Seyfert 2 galaxies, in fact, generally show nearly zero or even slightly positive  $\Delta V$  values, consistent with the results of Sarzi et al. (2016), and also with what we find when cross-correlating the Best & Heckman catalogue with our control sample.

In summary, only a few dozen Seyfert 2 galaxies show kpc-scale cold-gas outflows among the nearly complete sample of almost 10,000 SDSS galaxies that we have analysed. Furthermore, although nearly a third of these outflowing systems feature some of the most luminous of our Seyfert 2 nuclei, both the IR luminosity and the nature of the radio emission in our Seyfert 2 galaxies indicates that star-formation may be powering an even higher fraction of the NaD-outflows observed in the Seyfert 2 population.

## 5 CONCLUSIONS

Using SDSS DR7 data and the value-added catalogues of [Oh et al. \(2011, 2015\)](#), we have selected a nearly complete sample of  $\sim 10,000$  nearby ( $z < 0.2$ ) Seyfert 2 galaxies, and investigated the kinematics of their cold-gas medium at kpc-scales, as traced by interstellar NaD absorption lines. In order to set a detection threshold for possible cold-gas outflows and draw conclusions on the incidence of AGN-driven outflows in the nearby Universe, we have also measured the properties of the interstellar NaD absorption in a carefully-selected sample of  $\sim 44,000$  control galaxies that match our Seyferts in redshift, luminosity, size, light concentration, apparent flattening, colour and morphological classification. Our main results are as follows:

- The incidence of detected NaD absorption across our Seyfert 2 and control samples are similar, being 5.7% and 4.9% in the two populations respectively. This is particularly important, as it allows for a direct comparison between the cold-gas kinematics found across these two galaxy populations.
- Out of 9859 Seyfert 2 galaxies, only 53 show evidence of kpc-scale cold-gas outflows. Even accounting for inclination biases against the detection of NaD-outflowing systems, this result strongly suggests that optical AGN activity cannot be important in driving galactic winds capable of quenching star-formation in the nearby Universe.
- The overall cold-gas kinematic behavior traced by the NaD interstellar absorption in Seyfert 2 and control galaxies (as shown in the  $V_{\text{NaD}} - V_{\star}$  versus  $\sigma_{\text{NaD}} - \sigma_{\star}$  diagrams) is rather similar, and the presence of an optical AGN does not boost the fraction of NaD outflows compared to the control sample, where such outflows are likely driven by star-formation. In fact, the incidence of NaD outflows among Seyfert 2s is actually lower, being 9% of NaD-detected objects, compared to 16% for the control sample.
- Consistent with previous studies, many NaD-outflowing Seyfert 2 galaxies are some of the brightest AGN ( $\log L_{[\text{O III}]}$   $> 42.3 \text{ erg s}^{-1}$ ). However, this only accounts for 32% of the outflows detected in Seyfert 2s.
- On the other hand, ancillary radio and IR data of our Seyferts (available for 19% and 55% of the objects with interstellar NaD absorption) suggests that star-formation is likely to be the bigger contributor to the observed NaD-outflows. Among the NaD-outflowing systems with radio or IR measurements, around 90% show radio emission consistent with being powered by star formation rather than AGN activity, and 55% show IR luminosity consistent with a LIRG or ULIRG classification. That a similar behaviour is observed across our control sample further indicates that

star formation is the principal driver of many of the outflows observed in our Seyfert 2 galaxies.

The negligible fraction of Seyferts found to host outflows in this work reinforces the conclusions of recent studies (e.g. [Kaviraj et al. 2015](#); [Sarzi et al. 2016](#)), which have suggested that the long time delay between the onset of star formation and the triggering of the AGN hinders the ability of the AGN to strongly regulate star formation activity. In essence, the gas reservoir is significantly depleted before the AGN is triggered, so that the AGN acts largely to mop up residual gas in the system, rather than influencing the bulk of the star formation episode. It is worth noting again that, since these papers have studied galaxies outside clusters, this scenario operates in low-density environments (which, nevertheless, host the vast majority of galaxies) at low redshift. As discussed in the introduction, the coupling between AGN and their hosts is stronger in clusters, and since performing similar NaD analyses at high redshift is difficult, drawing conclusions about low-density environments in the early Universe is currently unfeasible.

While our results, combined with the recent literature, suggests that optical AGN activity may not play a significant role in quenching star formation in the nearby Universe, future integral-field observations, possibly assisted by adaptive optics, may shed further light on the relative role of AGN and star formation in powering the kpc-scale cold-gas outflows found in Seyfert 2 galaxies. It is worth noting, in this context, that the [O III] luminosity distribution of our Seyfert 2 sample extends to the more typical values observed in Seyfert 1 systems. Hence, even though the measurement of NaD outflows in these objects is generally hampered, either by the presence of a non-thermal continuum, or by a real absence of neutral Sodium along the line of sight, it appears unlikely that Seyfert 1s could power many more kpc-scale cold-gas outflows, just on the basis that their engines could possibly be more powerful than the AGN probed in this study. On the other hand, it also remains to be established how frequently the ionised-gas outflows often found in nearby Type 1 AGN (e.g., [Perna et al. 2017](#)) really extend to kpc scales, again, for instance, through the use of integral-field spectroscopy (e.g., [Cresci et al. 2015](#)).

Integral-field observations may also clarify the impact of shocks on the nebular emission that is observed in most of the NaD-outflowing galaxies in our control sample, which very often shows composite AGN/star-forming activity and LINER-like emission. Indeed, if shocks do not always contribute to the observed nebular spectrum (as is the case in the study of [Ho et al. 2014](#)), this may leave some room for AGN, possibly during a very obscured phase ([Perna et al. 2017](#); [Harrison 2017](#)), to contribute to the outflows observed in our control sample and also in the more general galaxy population.

A further avenue of exploration is the role of mergers in driving inflows and outflows of cold gas. Deep surveys like the Stripe 82 and, in particular, new datasets that are both wide and deep (e.g. DECaLS and those further downstream like LSST ([Ivezic et al. 2008](#); [Abell et al. 2009](#); [Schlegel et al. 2015](#); [Blum et al. 2016](#))) are capable of revealing faint tidal features due to recent interactions (e.g. [Kaviraj 2014a,b](#)). Such data can be combined with the NaD

analysis presented here to elucidate the role of merging in triggering galactic-scale outflows in the nearby Universe.

Nevertheless, to conclude, the results from this study suggest that galactic-scale outflows at low redshift are no more frequent in Seyferts than they are in similar non-active galaxies, that optical AGN are not significant contributors to the quenching of star formation in the nearby Universe and that star formation may be the principal driver of outflows even in systems that host an AGN.

## 6 ACKNOWLEDGEMENTS

Both BN and MS acknowledge the financial support and hospitality provided by the European Southern Observatory (ESO) through the award of an ESO studentship and visiting fellowship, respectively. SK acknowledges a Senior Research Fellowship from Worcester College Oxford. This work would not have been possible without the data taken from the Sloan Digital Sky Survey (SDSS), the SDSS added-value OSSY emission-line catalogue and the contribution of large numbers of citizen scientists towards classifying the morphology of SDSS galaxies.

## REFERENCES

- Abazajian K. N., et al. 2009, *ApJS*, **182**, 543
- Abell P. A., et al. 2009, arXiv preprint arXiv:0912.0201
- Baldwin J. A., Phillips M. M., Terlevich R., 1981, *PASP*, **93**, 5
- Belfiore F., et al. 2016, *MNRAS*, **461**, 3111
- Best P. N., Heckman T. M., 2012, *MNRAS*, **421**, 1569
- Binney J., 2004, *MNRAS*, **347**, 1093
- Binney J., Tabor G., 1995, *MNRAS*, **276**, 663
- Blum R. D., et al. 2016, in American Astronomical Society Meeting Abstracts. p. 317.01
- Bruzual G., Charlot S., 2003, *MNRAS*, **344**, 1000
- Cappellari M., Emsellem E., 2004, *PASP*, **116**, 138
- Cardoso L. S. M., Gomes J. M., Papaderos P., 2017, preprint, ([arXiv:1705.04224](https://arxiv.org/abs/1705.04224))
- Chen Y.-M., Tremonti C. A., Heckman T. M., Kauffmann G., Weiner B. J., Brinchmann J., Wang J., 2010, *AJ*, **140**, 445
- Cicone C., et al. 2014, *A&A*, **562**, A21
- Cid Fernandes R., Stasińska G., Schlickmann M. S., Mateus A., Vale Asari N., Schoenell W., Sodr e L., 2010, *MNRAS*, **403**, 1036
- Cid Fernandes R., Stasińska G., Mateus A., Vale Asari N., 2011, *MNRAS*, **413**, 1687
- Cresci G., et al. 2015, *A&A*, **582**, A63
- Croton D. J., et al. 2006, *MNRAS*, **365**, 11
- Ellison S. L., Teimoorinia H., Rosario D. J., Mendel J. T., 2016, *MNRAS*, **455**, 370
- English W., Hardcastle M. J., Krause M. G. H., 2016, *MNRAS*, **461**, 2025
- Fabian A. C., 2012, *ARA&A*, **50**, 455
- Fujita A., Martin C. L., Mac Low M.-M., New K. C. B., Weaver R., 2009, *ApJ*, **698**, 693
- Gitti M., Brighenti F., McNamara B. R., 2012, *Advances in Astronomy*, **2012**, 950641
- Harrison C., 2017, preprint, ([arXiv:1703.06889](https://arxiv.org/abs/1703.06889))
- Harrison C. M., Alexander D. M., Mullaney J. R., Swinbank A. M., 2014, *MNRAS*, **441**, 3306
- Heckman T. M., Lehnert M. D., Strickland D. K., Armus L., 2000, *ApJS*, **129**, 493
- Ho L.-T., et al. 2014, *MNRAS*, **444**, 3894
- Ivezic Z., et al. 2008, arXiv preprint arXiv:0805.2366
- Jeong H., Sukyoung K. Y., Kyeong J., Sarzi M., Sung E.-C., Oh K., 2013, The Astrophysical Journal Supplement Series, 208
- Kauffmann G., et al. 2003, *MNRAS*, **346**, 1055
- Kaviraj S., 2014a, *MNRAS*, **437**, L41
- Kaviraj S., 2014b, *MNRAS*, **440**, 2944
- Kaviraj S., Schawinski K., Silk J., Shabala S. S., 2011, *MNRAS*, **415**, 3798
- Kaviraj S., Shabala S. S., Deller A. T., Middelberg E., 2015, *MNRAS*, **452**, 774
- Kaviraj S., et al. 2017, *MNRAS*, **467**, 4739
- Kewley L. J., Dopita M. A., Sutherland R. S., Heisler C. A., Trevena J., 2001, *ApJ*, **556**, 121
- King A., Pounds K., 2015, *ARA&A*, **53**, 115
- Kormendy J., Ho L. C., 2013, *ARA&A*, **51**, 511
- Krumholz M. R., Thompson T. A., Ostriker E. C., Martin C. L., 2017, preprint, ([arXiv:1702.05102](https://arxiv.org/abs/1702.05102))
- LaMassa S. M., Heckman T. M., Ptak A., Urry C. M., 2013, *ApJ*, **765**, L33
- Lamastra A., Bianchi S., Matt G., Perola G. C., Barcons X., Carrera F. J., 2009, *A&A*, **504**, 73
- Li Y., Bryan G. L., Ruszkowski M., Voit G. M., O'Shea B. W., Donahue M., 2015, *ApJ*, **811**, 73
- Lintott C., et al. 2011, *MNRAS*, **410**, 166
- Martin C. L., 2005, *ApJ*, **621**, 227
- Masters K. L., et al. 2010, *MNRAS*, **404**, 792
- Nyland K., et al. 2013, *ApJ*, **779**, 173
- O'Mill A. L., Duplancic F., Garc a Lambas D., Sodr e Jr. L., 2011, *MNRAS*, **413**, 1395
- Oh K., Sarzi M., Schawinski K., Yi S. K., 2011, *ApJS*, **195**, 13
- Oh K., Yi S. K., Schawinski K., Koss M., Trakhtenbrot B., Soto K., 2015, *ApJS*, **219**, 1
- Park J., Jeong H., Yi S. K., 2015, *ApJ*, **809**, 91
- Perna M., Lanzuisi G., Brusa M., Mignoli M., Cresci G., 2017, preprint, ([arXiv:1703.05335](https://arxiv.org/abs/1703.05335))
- Rupke D. S., Veilleux S., Sanders D. B., 2002, *ApJ*, **570**, 588
- Rupke D. S., Veilleux S., Sanders D. B., 2005a, *ApJS*, **160**, 87
- Rupke D. S., Veilleux S., Sanders D. B., 2005b, *ApJS*, **160**, 115
- Sarzi M., et al. 2006, *MNRAS*, **366**, 1151
- Sarzi M., et al. 2010, *MNRAS*, **402**, 2187
- Sarzi M., Kaviraj S., Nedelchev B., Tiffany J., Shabala S. S., Deller A. T., Middelberg E., 2016, *MNRAS*, **456**, L25
- Sato T., Martin C. L., Noeske K. G., Koo D. C., Lotz J. M., 2009, *ApJ*, **696**, 214
- Scannapieco E., Silk J., Bouwens R., 2005, *ApJ*, **635**, L13
- Scannapieco C., et al. 2012, *MNRAS*, **423**, 1726
- Schawinski K., 2012, preprint, ([arXiv:1206.2661](https://arxiv.org/abs/1206.2661))
- Schawinski K., Thomas D., Sarzi M., Maraston C., Kaviraj S., Joo S.-J., Yi S. K., Silk J., 2007, *MNRAS*, **382**, 1415
- Schlegel D. J., et al. 2015, in American Astronomical Society Meeting Abstracts. p. 336.07
- Shabala S. S., Deller A., Kaviraj S., Middelberg E., Turner R. J., Ting Y. S., Allison J. R., Davis T. A., 2017, *MNRAS*, **464**, 4706
- Shimasaku K., et al. 2001, *AJ*, **122**, 1238
- Silk J., Rees M. J., 1998, *A&A*, **331**, L1
- Singh R., et al. 2013, *A&A*, **558**, A43
- Strateva I., et al. 2001, *AJ*, **122**, 1861
- Strauss M. A., et al. 2002, *AJ*, **124**, 1810
- Taghizadeh-Popp M., 2010, *PASP*, **122**, 976
- Untertorn C. T., Ryden B. S., 2008, *ApJ*, **687**, 976
- Veilleux S., Osterbrock D. E., 1987, *ApJS*, **63**, 295
- Villar Mart n M., Emonts B., Humphrey A., Cabrera Lavers A., Binette L., 2014, *MNRAS*, **440**, 3202
- Westoby P. B., Mundell C. G., Baldry I. K., 2007, *MNRAS*, **382**, 1541
- Yan R., Blanton M. R., 2012, *ApJ*, **747**, 61



This paper has been typeset from a  $\text{\TeX/L\AA\TeX}$  file prepared by the author.